Available online at www.sciencedirect.com
SCIENCE DIRECT®
Pergamon
Cement and Concrete Research 33 (2003) 1013–1020
CEMENT AND CONCRETE RESEARCH

# Early development of properties in a cement paste: A numerical and experimental study

Antonio Principallo[a,*], Pietro Lura[b], Klaas van Breugel[b], Giovanni Levita[a]

[a]Department of Chemical Engineering, Industrial Chemistry and Materials Science, University of Pisa, Via Diotisalvi 2, Pisa 56126, Italy
[b]Stevin Laboratory, Concrete Structures Group, Faculty of Civil Engineering and Geosciences, Delft University of Technology, PO Box 5048, Delft 2600 GA, The Netherlands

Received 22 August 2002; accepted 13 December 2002

**Abstract**

This paper presents the results of an experimental and numerical study of the properties of a high-performance Portland cement paste (w/c ratio 0.37; 5% silica fume) cured at 20 °C in sealed conditions for 5 days. Properties such as electrical conductivity, strength, stiffness, porosity, Vicat penetration, and autogenous deformation were measured and modelled. The kinetics of hydration was studied by means of isothermal calorimetry. The numerical simulations were performed with CEMHYD3D, developed at the National Institute of Standards and Technology, and HYMOSTRUC, developed at the Delft University of Technology. The results of the simulations were compared with experimental data, and the match was good. Clear correlations were found among electrical conductivity, autogenous shrinkage, and connectivity of solids.


*Keywords:* Portland cement; Modelling; Electrical properties; Mechanical properties; Shrinkage

## 1. Introduction

In high-performance concretes, low water-to-cement ratios lead to a significant self-desiccation during hydration [1]. The presence of silica fume further increases this effect—the principal causes being the refinement of the pore structure and the pozzolanic reaction [2]. Although the real mechanism of autogenous shrinkage is not yet fully understood, experimental correlations were found between changes of the relative humidity in the pores and volume contraction [3]. Capillary phenomena, changes in surface tension, and disjoining pressure were already considered by Powers [4]. More recently, autogenous shrinkage was calculated on the basis of different mechanisms [5–7].

The autogenous shrinkage increases for months [8]; most of it, however, takes place in the first few days. Since the contraction of the cement paste is constrained by rigid aggregates, internal stresses [9] and bulk deformation [10–12] occur.

Measurements of electrical conductivity provide a non-destructive technique to monitor the development of hydration in cement-based materials. Electrical monitoring is based on the assumption that in a system undergoing physical and chemical changes, the electrical parameters reflect the variations in nature, mobility, concentration, and distribution of the charge carriers, and of the dipolar species associated with these changes [13]. In particular, the amount of water and its interactions with the matrix have a significant influence on the dielectric response [14]. Similarly to shrinkage, variations in the electrical properties of cement mixtures occur for several months after casting [15,16], although most of them take place in a few days.

By monitoring the electrical conductivity, it is possible, with the help of experimental and theoretical correlations, to evaluate the degree of hydration of the cement [14]. By means of analytical [17] or numerical models [6,18], the development of stiffness, strength, and shrinkage can be derived.

In this paper, results of a series of experiments performed on a cement paste are presented together with numerical simulations of the hydration process and of the development of microstructure. The main aim of this study was to

* Corresponding author. Tel.: +39-50-511-201; fax: +39-50-511-266.
*E-mail address:* levita@ing.unipi.it (A. Principallo).

0008-8846/03/$ – see front matter © 2003 Elsevier Science Ltd. All rights reserved.
doi:10.1016/S0008-8846(03)00002-4

compare experimental data with the results of two recent predictive models, which are based on rather different basic assumptions. Both models satisfactorily agreed with experiments. Correlations between electrical conductivity and autogenous shrinkage were also found.

## 2. Materials and methods

### 2.1. Cement paste

A Type I Portland cement (CEM I 52.5 R; ENCI) was used. The mineral composition of the cement is shown in Table 1. The water-to-cement ratio (w/c) was 0.37. Further additives were silica fume (in slurry form), a lignosulphonate-based plasticizer, and a naphthalene sulphonate-based superplasticizer. Mix compositions are reported in Table 2.

### 2.2. Isothermal calorimetry

The thermal power dissipated in isothermal conditions was measured at 20 °C with an isothermal calorimeter (3114/3236; TAM Air), on 10-g samples. Tests were duplicated.

### 2.3. Vicat penetration test

Setting was measured with an automatic Vicat needle apparatus (MATEST). Measurements were performed according to the UNI standard; readings were taken every 10 min.

### 2.4. Electrical conductivity

Electrical conductivity was measured with the apparatus CONSENSOR [14]. The sensor consisted of two cylindrical rods (10 mm in diameter) placed at an axial distance of 30 mm. The device was controlled by a microchip that allowed continuous measuring. The experimental setup is shown in Fig. 1. The cement paste was sealed and its temperature was kept at 20 ± 1 °C by means of a cooling system. Measurements started about 10 min after mixing and were carried out for 5 days. Data were taken at 20 MHz to minimize polarization effects at the electrode/paste interface.

Table 1
Mineral composition of the cement (Type I, 52.5 R)

| | |
|---|---|
| CaO [%] | 64 |
| $SiO_2$ [%] | 21 |
| $Al_2O_3$ [%] | 5 |
| $Fe_2O_3$ [%] | 3 |
| MgO [%] | 2 |
| $SO_3$ [%] | 3.3 |
| Cl [%] | ~0.05 |
| Loss on ignition [%] | ~1 |
| Insoluble residue [%] | ~1 |
| $Na_2O$ equivalent [%] | 0.6 |

Table 2
Composition of the examined mix

| Component | Parts (by weight) |
|---|---|
| Cement, CEM I 52.5 R ENCI (Blaine, 530 $m^2$/kg) | 100 |
| Microsilica, slurry (Heidelberger Bauchemie) dry content: 51% (BET, 19,000 $m^2$/kg) | 10.5 |
| Napthalene sulphonate (Addiment FM951 NBC Bouwstoffen) dry extract: 40% | 1.7 |
| Lignosulphonate (Addiment BV1 NBC Bouwstoffen) dry extract: 36% | 0.2 |
| Total water | 37 |

### 2.5. Autogenous shrinkage

The free deformations of the sample were measured with an autogenous deformation testing machine (ADTM) [7], shown in Fig. 2. The paste was cast in a prismatic steel mould (4 × 15 × 100 $cm^3$) whose internal surface was lined with a Teflon layer to minimize friction with the sample. A cooling liquid was circulated on the outer surface of the mould. The shrinkage was evaluated by measuring the movements of two steel bars, at the beginning 750 mm apart, solidly connected to the cast and emerging from the mould. The position of each bar was detected by linear variable differential transducers. Readings were taken for 5 days. The test was duplicated with good repeatability (within 3%).

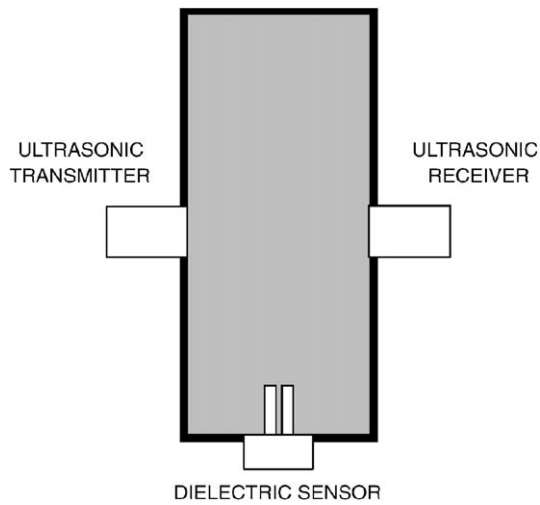


Fig. 1. Experimental setup for the simultaneous measurements of electrical conductivity (front electrode) and ultrasonic wave propagation (side transducers). Mold size: 20 × 20 × 30 $cm^3$.

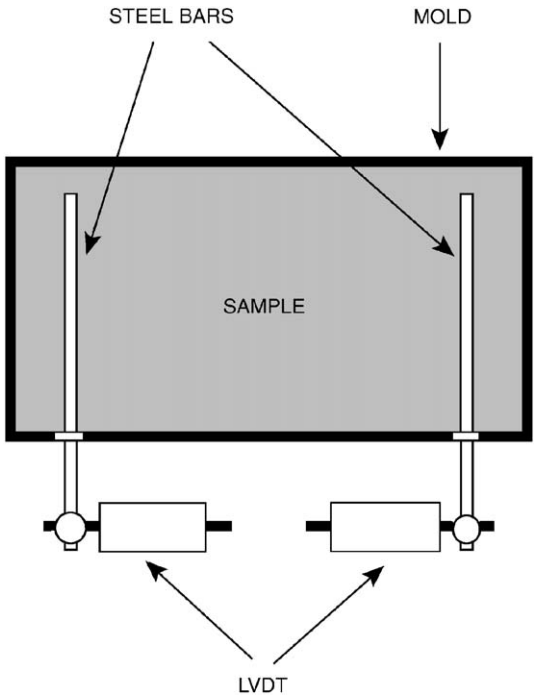


Fig. 2. Experimental setup for detecting autogenous shrinkage. The horizontal movements of two steel rods embedded in the specimen are revealed by two LVDTs. Mold size: $4 \times 15 \times 100$ cm$^3$.

### 2.6. Compressive strength and elastic modulus

The compressive strength and the Young's modulus were measured on samples ($150 \times 150 \times 150$ and $50 \times 50 \times 200$ mm$^3$, respectively) of different ages. Samples were cast in temperature-controlled steel moulds and kept at 20 °C in sealed conditions.

## 3. Numerical analysis

### 3.1. General

Several models have been proposed to describe the evolution in time of the hydration and of the microstructure of a cement paste. When only the advancement of hydration needs to be described, models based on overall kinetics are sufficient, in which microscopic features are accounted for by adjustable parameters, as in the Avrami–Erofeef equation [18].

If a more detailed description is needed, a *particle kinetics* approach is to be preferred, in which individual particles are assumed to react independently. In this approach, for instance, the effect of the particle size of cement grains on the overall hydration kinetics can be considered. Finally, models based on *integrated kinetics* explicitly account for the influence of the particle interaction on the formation of the microstructure and on the rate of hydration. Two of such models, namely CEMHYD3D (NIST) [19] and HYMOSTRUC (TU Delft) [18], were used in the present study.

### 3.2. CEMHYD3D

CEMHYD3D can be classified among the so-called digital image-based models. These models operate at the subparticle level; each cement particle is represented as a collection of elements (pixels). Hydration is simulated by operating on the pixels using a set of cellular automata-like rules [20]. The random movement of ions is intrinsically modeled and so is the complete dissolution of the fine cement particles. Properties such as percolation, diffusivity, and setting are easily computable from the three-dimensional hydrated structure. Self-desiccation is simulated by emptying the capillary pores as hydration proceeds [21]. The evolution of pixels is organized in cycles, where each cycle is made of dissolution, diffusion, and reaction steps. The evolution of the system is given in terms of elapsed cycles. To correlate number of cycles and hydration time, a calibration is required by comparison with experiments. The following relationships holds between hydration time $t$ and number of cycles: $t = B$ cycles$^2$.

### 3.3. HYMOSTRUC

In this model, the cement particles are modelled as spheres of different diameters. The hydration proceeds at the particle/water interface and the hydration products grow as concentric spherical shells around the original particles. Distinction is made between inner and outer products. The transition from a phase boundary-controlled reaction regime to a diffusion-controlled one (determined by the shell thickness of the hydration products) is explicitly accounted for.

The model enables the prediction of the hydration level as a function of the chemical composition of the cement, of the particle size distribution (PSD), and the water-to-cement ratio [18].

The effect of the temperature on the physical properties of the cement paste is also taken into account. Additionally, the model allows to examine the aggregate–paste interfacial transition zone [6], the development of the elastic modulus [22], the early age creep [22], and the autogenous shrinkage of both cement paste and concrete [6].

## 4. Results and discussion

### 4.1. Degree of hydration

The PSD of the cement was measured with a laser analyser and approximated by the Rosin–Rammler distribution [18]. The content of $C_3S$ and $C_2S$ necessary to run HYMOSTRUC was obtained by Bogue calculation using data in Table 1. In CEMHYD3D, the cement was assumed to contain only $C_3S$. This approximation should cause only

minor difference [23], since the two silicates produce nearly the same volume of products. Moreover, $C_3S$ was the major constituent ($\sim$63%) of the cement considered. The pozzolanic reaction of silica fume was explicitly considered in the CEMHYD3D code, whereas in HYMOSTRUC, it was accounted for only indirectly by a refinement of the pore structure [6].

The degree of hydration was defined [18] as: $\alpha = Q(t)/Q_{pot}$, where $Q(t)$ is the heat generated at age $t$ and was obtained by integrating the thermal power given by the isothermal calorimeter (see curves in Fig. 3). $Q_{pot}$ is the potential heat at complete hydration, for which a value of 535 kJ/kg was estimated in Ref. [24]. The progress of hydration is shown in Fig. 4, along with the results of the numerical simulation. The calorimetric data were used to synchronise the numerical simulations; once this was done, the match between experiment and simulation was very good over the entire time span for both models. The hydration parameters found for the HYMOSTRUC code agreed with those previously found [18]. The time constant $B$ for the NIST code was $4.37 \times 10^{-4}$ h/cycles$^2$.

### 4.2. Hydration and development of the microstructure

Once the two codes were synchronised with the calorimetric data, it was possible to examine the hydration in detail. For instance, it was possible to account for the influence of particle size on the rate of hydration. Since the reaction with water occurs at the particle/fluid interface (or its immediate vicinity), the reaction rate increases with particle fineness. This is clearly described in Fig. 5, which shows that, approximately, the isochronous degree of hydration linearly depends on particle size on a logarithmic scale. The two codes yielded similar results. Once the kinetics of each particle, and related volume stoichiometry, could be described, it was possible to model the evolution of the microstructure, taking into account the local arrangements of neighbouring particles. In this way, pictorial representations of the system, at fixed hydration levels, could be

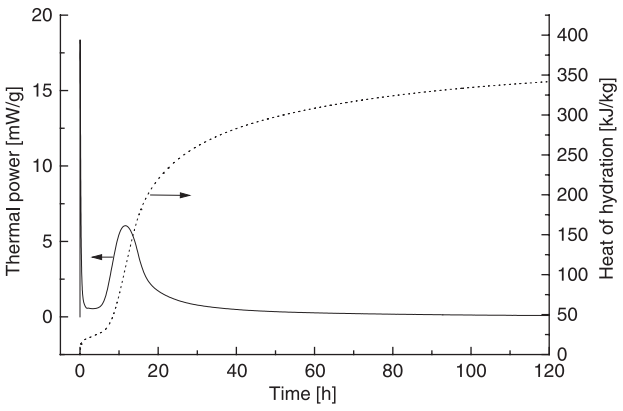


Fig. 3. Specific thermal power dissipated in isothermal conditions (20 °C) and cumulative heat of hydration (by integration of the power data).

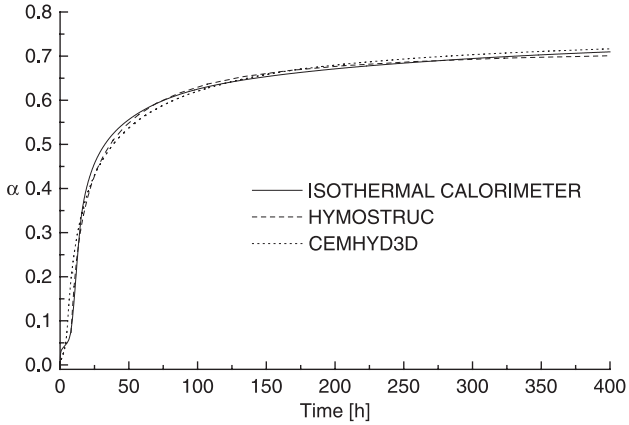


Fig. 4. Comparison of experimental hydration kinetics (from calorimetric data) and numerical simulations.

obtained. These graphical results were compared with scanning electron microscopy (SEM) images of the paste. In Fig. 6, we compare a SEM back-scattered electron (BSE) image of a 1-day-old sample ($\alpha \approx 0.45$) with computed images generated by sectioning with a plane the three-dimensional arrays of solid particles.

The pictures cover an area of about $70 \times 70$ μm$^2$. In both simulations, the cement grains were modeled as spheres; the SEM image, of course, describes the real shape of cement grains. By examining the images, it is possible to appreciate a basic difference between the two codes. In HYMOSTRUC, the reaction products form and stay at the solid–liquid interface so that the hydration proceeds radially, outwards and inwards, forming spherical layers around unhydrated particle cores. On the contrary, in the CEMHYD3D code hydration products (C–S–H and CH) can appear anywhere in the available interparticle space as well as on the particle surface, including the surface of hydration products.

Fig. 6 makes clear how the porosity develops: the original continuous liquid phase breaks in islands as a result of the increase of the volume of solids and the decrease of water. Depending on the initial water-to-cement ratio, the pores can be partially filled with residual water. It must be

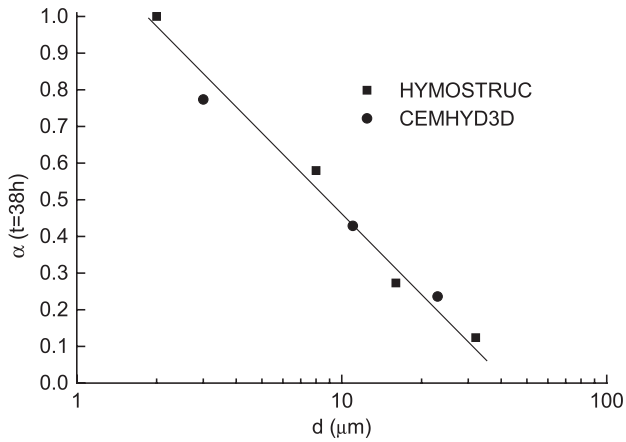


Fig. 5. Effect of particle size on isochronous (38 h) degree of hydration.

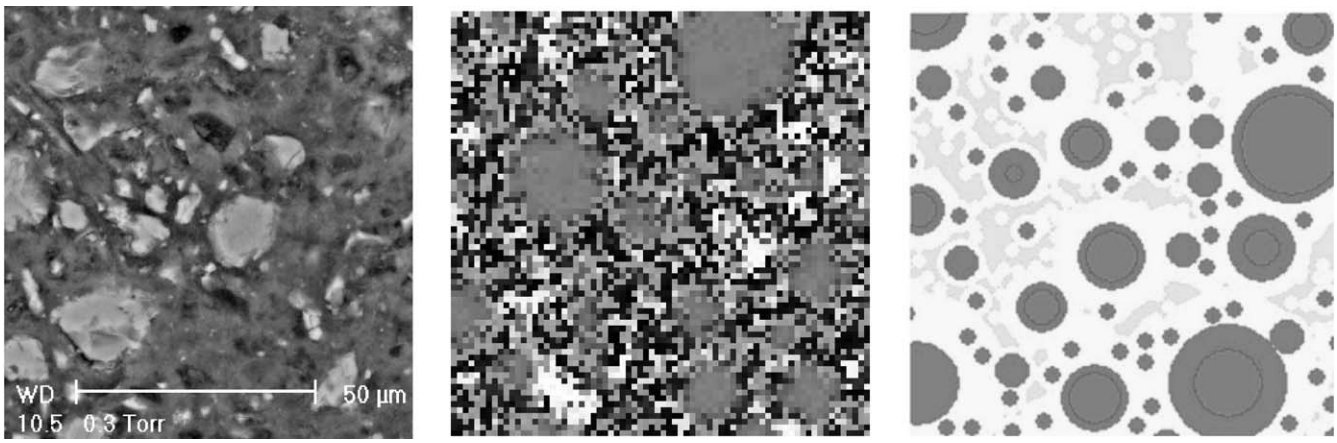


Fig. 6. SEM (back-scattered electrons) image of the cement paste after 1-day cure (left) and two-dimensional sections generated by three-dimensional modelling (middle: CEMHYD3D; right: HYMOSTRUC).

pointed out that the two-dimensional representation shown in Fig. 6 can be misleading. The loss of long-range continuity (depercolation) of an initially continuous phase occurs at rather different volume fractions depending on the dimensionality of the system: ~0.16 for a three-dimensional random array and ~0.45 for a two-dimensional distribution. When the liquid phase depercolates, the residual water is contained into rather large, yet isolated, pores. As the hydration goes on, both the total volume of voids (porosity) and their average size decrease as hydration proceeds. Both models gave a satisfactory description of the porosity evolution. However, HYMOSTRUC is not suited, at the present time, to account for the presence of solids other than cement particles, whereas in CEMHYD3D, the addition of silica fume can be simulated by introducing into the space model a suitable number of one-pixel large elements. Consequently, the total porosity reckoned with HYMOSTRUC differed from that given by CEMHYD3D by the volume of the filler (Fig. 7). If the volume of silica fume is added to the pore volume given by CEMHYD3D, the two models will be equivalent (Fig. 7). The values of the empty porosity given by the two models substantially coincided because the two codes worked on formulations whose initial volume fractions of solids were the same. The final value of the empty porosity calculated by the models (~6%) agreed with literature data [24].

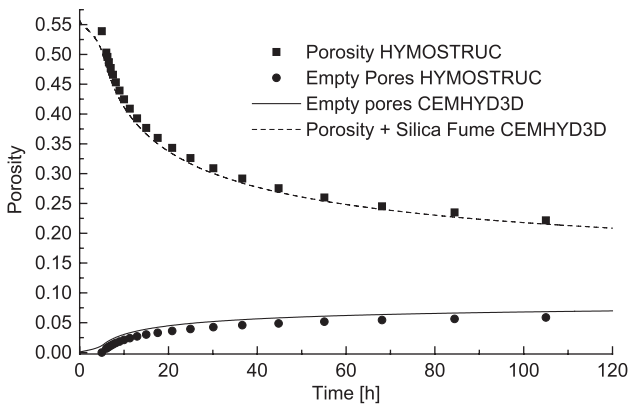


Fig. 7. Time evolution of the total (top) and empty porosity (bottom) according to HYMOSTRUC and CEMHYD3D codes.

### 4.3. Mechanical properties

Once the connectivity of the solid phase in the cement paste has been first attained, the development of strength is essentially related to the decrease of porosity. For this reason, Powers and Brownyard [25] introduced the gel-to-space ratio ($X$) concept, and verified that the compressive strength of mortars and concrete follows the equation:

$$R = R_0 X^3$$

where $X$ is the ratio of the volume of the hydration products to the space available for their growth; and $R_0$ represents the maximum compressive strength that might be reached if all the capillary pores were filled by hydration products. The value of $R_0$ depends on the cement, water-to-cement ratio, and curing conditions [25]. In this work, by means of a fitting procedure, we found that $R_0 = 138$ MPa.

The accuracy of Powers' relationship was confirmed by the numerical simulations. Once the kinetics of the hydration (see Fig. 4) and the volume stoichiometry have been known, it is possible to implement Powers' relationship into the NIST code and to describe the time evolution of the compressive strength. As one can see in Fig. 8, the agreement of simulation with experiments was very satisfactory.

An attempt was made to analyse the strength development in a different way. Since the fluid paste starts solidifying when the initially isolated solid particles adhere to one another, we looked at the extensions of interparticle contacts as a parameter that gives an indication of the efficiency of the consolidation of the system. In fact, the development of strength and stiffness of hardening cement-based materials can be attributed to the increasing interactions between hydrating particles, in particular to the num-

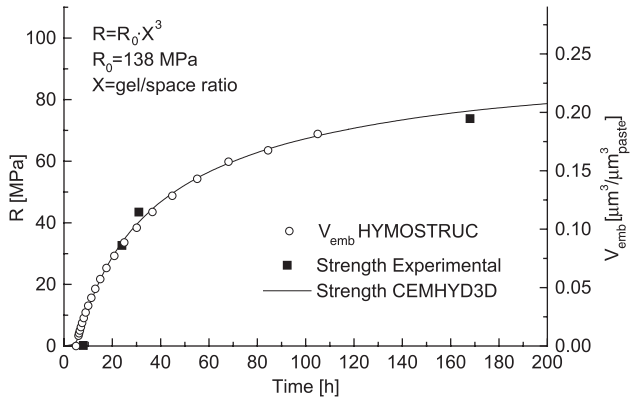


Fig. 8. Comparison of experimental strength and predictions from CEMHYD3D following Power's relationship. Also shown is the computed embedded cement volume.

ber of contact points between them [18]. If two neighbouring particles were initially located at a distance less that the sum of their radii after hydration, the particles would overlap. Predictions of the strength by HYMOSTRUC follow the "embedded cement" concept [18]. The extent of the overlap region (embedded volume, $V_{emb}$) depends on the pristine distance and extent of hydration. Both quantities are calculated by the HYMOSTRC code. Computed values of $V_{emb}$ are shown in Fig. 8; they closely replicate the mechanical data so that the strength can be described as:

$$R = kV_{emb}$$

Lokhorst [22] proposed a model for the elastic modulus of concrete (bar model) based on an aggregate–element in series and in parallel with two paste elements. The development of the elastic modulus in the paste elements follows the degree of hydration. Also in this case, the agreement with experiment was good (Fig. 9).

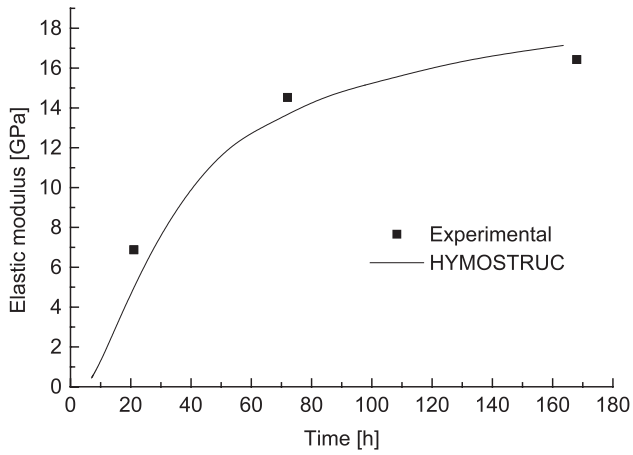


Fig. 9. Comparison of experimental elastic modulus and predictions from HYMOSTRUC following Lokhorst [22].

### 4.4. Vicat penetration

The Vicat test has been traditionally used to measure the set time of cement pastes. Topologically, this event is described in terms of percolation of solids. When setting occurs, a percolating pathway of connected solids forms throughout the cement paste volume [26]. We computed, with the CEMHYD3D model, the amount of connected solids at various elapsed times. The results are shown in Fig. 10 along with the normalised Vicat penetration data. When the topological set point is reached, the amount of connected solids rises abruptly and so does the normalised needle penetration depth; this supports the interpretation of the set point in terms of topological transitions. In reality, a certain level of consolidation is required for the paste to resist the needle penetration, so that the set point occurs with a certain delay with respect to the topological transition. The numerical results are quite satisfactory, especially when one is aware of the difficulties of modelling the dormant stage.

### 4.5. Electrical conductivity and autogenous shrinkage

The properties so far considered have dealt with the evolution of the solid constituents of the system (i.e., CSH, CH, and unhydrated cement). However, other important properties (for instance the tendency towards volume contraction during hydration) seem to depend on the properties of the pore fluids. Also the electrical conductivity depends on the amount, distribution, and composition of the residual water.

Autogenous shrinkage appears soon after setting, in some cases following a limited expansion. At setting, a solid skeleton forms in the paste. As water is consumed by the chemical reactions, the solids grow and the capillary pores start to empty. The relative humidity in the pores drops and water–air menisci form [27], leading to capillary depression and ultimately to autogenous shrinkage [28]. This stage corresponds to the first critical point in Fig. 11. After an initial rapid shrinkage, the process slows down and the

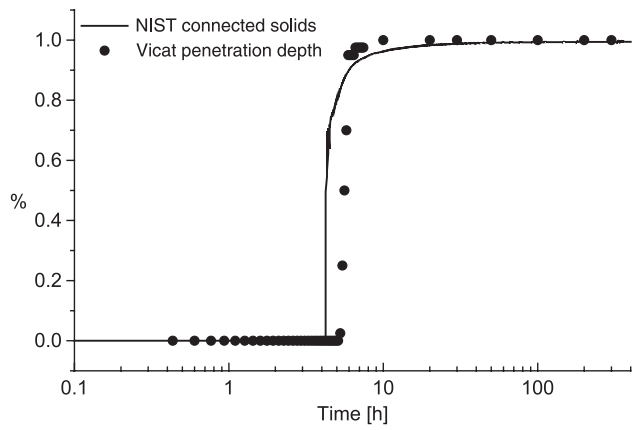


Fig. 10. Normalized Vicat penetration data and computed total amount of connected solids from CEMHYD3D.

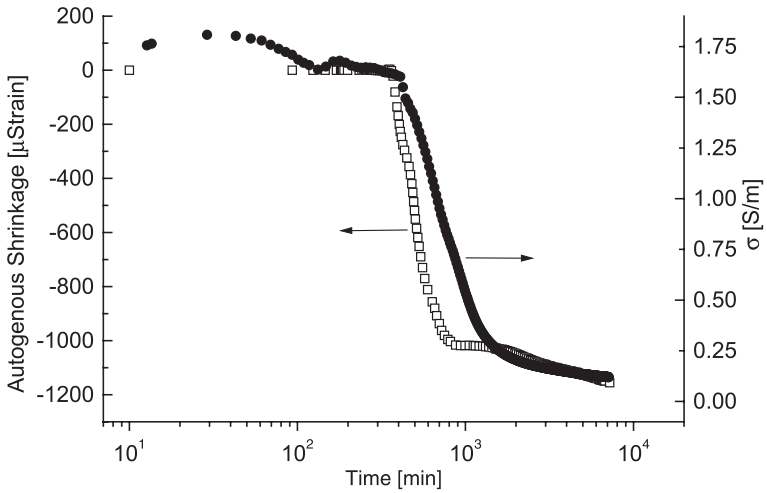


Fig. 11. Autogenous shrinkage (left axis) and electrical conductivity (right axis) as a function of time.

autogenous shrinkage occurs at a much lower rate. This second transition can be related to the depercolation of the pore phase. In fact, this phenomenon corresponds to a rapid increase of the elastic modulus of the cement paste (see Fig. 9) and the newly formed solid skeleton is now able to resist the capillary depression. There can be several reasons for the changing in shrinkage rate: (1) the progress of the hydration modifies the relative amount of solids and liquid; (2) the properties of the pore liquid (e.g., vapor pressure, surface tension) change; (3) the creep under the action of the hydrostatic stress generated by capillary phenomena; and (4) the increase in elastic modulus.

It is striking to note how closely the change in electrical conductivity resembles the evolution of the autogenous shrinkage. The drop of shrinkage and conductivity occur simultaneously, suggesting that both phenomena are strongly related.

At the very beginning, a slight increase in conductivity of cement pastes is typically observed [13], possibly associated with the heat evolution in the first hours (see also the calorimeter data in Fig. 3) and to the formation of a supersaturated solution. The drop in conductivity reflects the reduction and fragmentation of the pore phase filled with a water solution whose ionic composition changes with time. After the first drop, the reduction of conductivity occurred at a much lower rate. This was attributed to the depercolation of porosity [26] since only the water-filled connected pores represent the main pathway for the migration of charge carriers.

## 5. Conclusions

The evolution of the microstructure of a high-performance cement paste (w/c 0.37; 5% silica fume) was computed with two numerical codes, HYMOSTRUC and CEMHYD3D. The models were synchronised with experiments by matching the computed hydration kinetics with that obtained by isothermal calorimetry. The numerical analysis was very useful in describing the evolution of the porosity of the system and of the related physical properties such as electrical conductivity, autogenous shrinkage, and strength.

Also the effect of particle size on the chemical reactivity could be accurately described. A strict similarity between autogenous shrinkage and electrical conductivity was found, which confirms that the pore dynamics is the common origin of the mechanical and electrical behaviours of cement. It is believed that numerical codes can be of much help in developing new formulations and in gaining a deeper insight into the microstructure of cementitious materials.

## Acknowledgements

The authors would like to thank Mr. Ye Guang for helping with the modelling and Mr. J. Bisschop (Microlab, TU Delft) for the SEM picture. The assistance of Mr. E. Horeweg, Mr. A. van Rhijn, Mr. R. Mulder, and Mr. F.P.J. Schilperoort in performing the experiments is gratefully acknowledged.

## References

[1] B. Persson, G. Fagerlund (Eds.), International Research Seminar on Self-Desiccation and Its Importance in Concrete Technology, Lund, Sweden, June 10, 1997, Report TVBM-3075, Lund University, 1997.
[2] O. Mejlhede Jensen, Autogenous deformation and RH-change—self-desiccation and self-desiccation shrinkage (in Danish), PhD Thesis, Building Materials Laboratory, The Technical University of Denmark, TR 284/93, May 1993.
[3] O. Mejlhede Jensen, P. Freisleben Hansen, Autogenous deformation and change of the relative humidity in silica fume-modified cement paste, ACI Mater. J. 93 (6) (1996) 539–543.
[4] T.C. Powers, Mechanisms of shrinkage and reversible creep of hardening cement paste, Proceedings of the International Symposium on Structure of Concrete and Its Behaviour Under Load, Cement and Concrete Association, London, 1965, pp. 319–344.

[5] C. Hua, P. Acker, A. Erlacher, Analyses and models of the autogenous shrinkage of hardening cement paste: I. Modelling at macroscopic scale, Cem. Concr. Res. 25 (1995) 1457–1468.
[6] E.A.B. Koenders, Simulation of volume changes in hardening cement-based materials, PhD Thesis, Delft University of Technology, Delft, 1997.
[7] P. Lura, O.M. Jensen, K. van Breugel, Autogenous shrinkage in high-performance cement paste: An evaluation of basic mechanisms, Cem. Concr. Res., 2002.
[8] V. Baroghel-Bouny, A. Kheirbek, Effect of mix parameters on autogenous deformations of cement pastes—microstructural interpretations, Proceedings of the International RILEM Workshop Shrinkage of Concrete Shrinkage 2000, Paris.
[9] P. Golterman, Mechanical predictions on concrete deterioration: Part 1. Eigenstresses in concrete, ACI Mater. J. 91 (6) (1994) 543–550.
[10] E. Tazawa, S. Miyazawa, Autogenous shrinkage: What is understood and which are the further research needs? Proceedings of the International Workshop on Control of Cracking in Early-Age Concrete, Sendai, 2000.
[11] Ø. Bjontegaard, Thermal dilation and autogenous deformation as driving forces to self-induced stresses in high performance concrete, PhD Thesis, NTNU Division of Structural Engineering, 1999.
[12] P. Lura, K. van Breugel, I. Maruyama, Effect of curing temperature and type of cement on early-age shrinkage of High Performance Concrete, Cem. Concr. Res. 31 (12) (2001) 1867–1872.
[13] G. Levita, A. Marchetti, G. Gallone, A. Principallo, G.L. Guerrini, Electrical properties of fluidified Portland cement mixes in the early stage of hydration, Cem. Concr. Res. 30 (2000) 923–930.
[14] A. van Beek, Dielectric properties of young concrete—non-destructive dielectric sensor for monitoring the strength development of young concrete, PhD Thesis, Delft University of Technology, Delft, 2000.
[15] P.R. Camp, S. Bilotta, Dielectric properties of Portland cement paste as a function of time since mixing, J. Appl. Phys. 66 (12) (1989) 6007–6013.
[16] P. Gu, J.J. Beaudoin, Dielectric behaviour of hardened cement paste systems, J. Mater. Sci. Lett. 15 (1996) 182–184.
[17] F. Rostásy, A. Gutsch, M. Laube, Creep and relaxation of concrete at early ages—experiments and mathematical modelling, Proceedings of the 5th International RILEM Symposium on Creep and Shrinkage of Concrete, Barcelona, 1993, pp. 453–458.
[18] K. van Breugel, Simulation of hydration and formation of structure in hardening cement-based materials, PhD Thesis, Technical University Delft, 1997.
[19] D.P. Bentz, 'CEMHYD3D: a three-dimensional cement hydration and microstructure development modelling package, version 2.0.' NISTIR 6485, U.S. Department of Commerce, April 2000 (available at http://ciks.cbt.nist.gov/monograph).
[20] D.P. Bentz, E.J. Garboczi, Percolation of phases in a three-dimensional cement paste microstructural model, Cem. Concr. Res. 21 (1991) 325–344.
[21] D.P. Bentz, K.A. Snyder, P. Stutzman, Microstructural modelling of self-desiccation during hydration, in: B. Persson, G. Fagerlund (Eds.), International Research Seminar on Self-desiccation and Its Importance in Concrete Technology, Lund, Sweden, 10 June 1997, Report TVBM-3075, Lund University, 1997.
[22] S.J. Lokhorst, Deformational behaviour of concrete influenced by hydration related changes of the microstructure, Research Report, Delft University of Technology, 1998.
[23] E.J. Garboczi, D.P. Bentz, Computer simulation of the diffusivity of cement-based material, J. Mater. Sci. 27 (1992) 2083–2092.
[24] A.M. Neville, Properties of Concrete, Longman, London, 1995.
[25] T.C. Powers, T.L. Brownyard, Studies of the physical properties of hardened Portland cement paste (nine parts), J. Am. Concr. Inst. 43 (October 1946 to April 1947).
[26] A. Principallo, G. Levita, A. Marchetti, G. Gallone, G.L. Guerrini, Advancements in modelling the development of microstructure in cement pastes. 7th European Conference on Advanced Materials and Processes, Rimini, June 10–14, 2001.
[27] L. Barcelo, S. Boivin, P. Acker, J. Toupin, B. Clavaud, Early age shrinkage of concrete: Back to the physical mechanism. Presented at UEF Conference Advances in Concrete and Cement, Mt-Tremblant, Canada, August, 2000.
[28] O. Mejlhede Jensen, P. Freisleben Hansen, Autogenous deformation and RH-change in perspective, Cem. Concr. Res. 31 (2001) 647–654.